Functional and Structural Characterization of 2B Viroporin Membranolytic Domains[†]

Silvia Sánchez-Martínez,[‡] Nerea Huarte,[‡] Rubén Maeso,[‡] Vanessa Madan,[§] Luis Carrasco,[§] and José L. Nieva*[,‡]

Unidad de Biofísica (CSIC-UPV/EHU) and Departamento de Bioquímica, Universidad del País Vasco, Aptdo. 644, 48080 Bilbao, Spain, and Centro de Biología Molecular (CSIC-UAM), Universidad Autónoma de Madrid, Canto Blanco, 28049 Madrid, Spain

Received May 27, 2008; Revised Manuscript Received August 4, 2008

ABSTRACT: Nonstructural 2B viroporin is an intracellularly produced pore-forming protein required for effective enteroviral and rhinoviral replication. The sequence of 2B displays two putative interconnected transmembrane domains, which are predicted to insert into the negatively charged membranes of target organelles forming an integral hairpin. The use of an overlapping peptide library that spanned the complete 2B sequence has recently allowed the mapping of the cell plasma membrane porating activity to the partially amphipathic, amino-terminal transmembrane domain (TM1, residues 35−55). We describe here that although the TM1 peptide was effective in permeabilizing uncharged membranes, it induced marginal lysis of anionic bilayers. In fact, only the peptide representing the highly conserved carboxy-terminal transmembrane domain (TM2, residues 59−82) reproduced the capacity of the full 2B protein to efficiently permeabilize bilayers made of anionic phospholipids. Insertion into lipid monolayers and circular dichroism determinations were, however, consistent with penetration of the TM1 helix into both anionic and zwitterionic membranes, while TM2 interacting with membranes assumed a mixture of conformations. Moreover, addition of TM1 strongly stimulated TM2-induced permeabilization of the anionic membranes. In combination, TM1 and TM2 formed a complex that had structural properties, including a high proportion of extended nonhelical secondary structure, that were distinct from those of the individual peptides. Finally, a comparison of antimicrobial and hemolytic activities further underscored the TM1 domain's cytolytic character. Overall, our data support the idea that the cytolytic activity of TM1 in the negatively charged cell endomembranes targeted by 2B viroporin requires the cooperation of both transmembrane domains.

Nonstructural 2B product is an intracellularly expressed pore-forming protein responsible for the cell membrane permeabilization phenomena observed during infection by certain picornaviruses such as entero- and rhinoviruses (*1, 2*). Individual expression of 2B, or its precursor 2BC, in mammalian cells induces permeabilization of several endomembrane systems, including the plasma membrane, the endoplasmic reticulum (ER), and the Gogi complex (*3*−*8*). Expressed 2B products have been localized to the ER and Golgi complex, and to a lesser extent to the plasma membrane (*2, 5, 7*−*9*). Thus, it has been postulated that 2B pores might play a regulatory role during infection by modulating calcium and proton homeostasis or altering the solute balance across the plasma membrane. Also sustaining the proposed membrane permeability regulatory activities, 2B expressed from an alphavirus replicon has recently been shown to localize in mitochondria (*10*). 2B alters the normal morphology of these organelles and induces release of apoptogenic cytochrome *c* therein.

The enterovirus and rhinovirus 2B sequences bear two potential transmembrane domains (TMDs)[1] interconnected through a short potential turn that are proposed to assemble into a helical hairpin membrane anchor (*6, 11*−*15*). The amino-terminal domain contains several Lys residues distributed with helical periodicity, which confers partial amphipathicity to the sequence in an α-helical conformation (*11, 14*). On the basis of the fact that synthetic peptides representing a single helix may retain the capacity of the parental polypeptide sequences to assemble ion channels and pores in membranes (*16*−*19*), we recently assayed an overlapping peptide library that spanned the complete 2B sequence for cell plasma membrane permeabilization (*20*). We found that the only peptide displaying 2B-like permeabilizing activity when added to cultured cells in the nanomolar concentration range was the one spanning the amino-terminal TMD (designated as TM1 in this work). The mechanism of pore formation at the plasma membrane by this peptide further supported the idea that 2B viroporin might function during infection as an intracellularly delivered cytolytic toxin (*20*).

However, in contrast to the monolayer facing the cell external medium, the cytofacial plasma membrane monolayer

[†] This study was supported by the Spanish Ministerio de Educación y Ciencia (Grant BFU 2005-0695/BMC to J.L.N. and Grant BFU2006-02182/BMC to L.C.) and the University of the Basque Country (042.310-13552/2001).

* To whom correspondence should be addressed. Phone: 34 94 601 3353. Fax: 34 94 601 3360. E-mail: gbpniesj@lg.ehu.es.

[‡] Universidad del País Vasco.

[§] Universidad Autónoma de Madrid.

[1] Abbreviations: CD, circular dichroism; LUV, large unilamellar vesicles; MBP, maltose-binding protein; PC, phosphatidylcholine; PI, phosphatidylinositol; PV, poliovirus; TMD, transmembrane domain.

10.1021/bi800997a CCC: $40.75 © 2008 American Chemical Society
Published on Web 09/12/2008

Table 1: Poliovirus 2B Overlapping Peptide Library

peptide[a]	sequence	PV-1 2B numbering
P1	GITNYIESLGAAFGSGFTQQIS	1−22
P2	DKITELTNMVTSTITEKLLKNLIK	23−46
P3 (TM1)	K-TITEKLLKNLIKIISSLVIIT-WKK	K-35−55-WKK
P4 (Turn)	KIISSLVIITRNYEDTTTVLAT	46−67
P5 (TM2)	KKK-EDTTTVLATLALLGCDASPWQWLR	KKK-59−82
P6	DASPWQWLRKKACDVLEIPYVIKQ	74−97

[a] The notations used in this work are in parentheses.

and the lipid bilayers surrounding 2B target organelles are all enriched with anionic phospholipids (*21*). Specifically, phosphatidylinositol (PI) accounts for the major fraction of the anionic glycerophospholipids present in the ER and Golgi complex, while phosphatidylcholine (PC) is the major uncharged species found in these membranes. It is therefore inferred that a major fraction of intracellularly produced 2B translocates into the negatively charged surfaces of membranes enriched with these phospholipids. Supporting this view, in previous work we demonstrated that a soluble and purified poliovirus (PV) 2B fused to maltose binding protein (MBP−2B) was capable of inducing anionic PI liposome permeabilization to low-molecular weight solutes but was inactive against electrically neutral PC vesicles (*13*). Thus, we concluded that the capacity of 2B viroporin to form stable, size-limited, nonselective pores at small doses in model membranes was modulated by the presence of a negatively charged polar headgroup.

A previous mutagenesis study of the coxsackievirus 2B protein by van Kuppeveld and co-workers demonstrated that each of the two predicted TMDs could mediate membrane binding individually (*15*). However, the presence of the both domains was required for the 2B membrane permeabilizing activity, suggesting that the two TMDs are cooperatively involved in the formation of a membrane−integral 2B complex. In this work, we have used a complementary peptide approach to analyze the functional role of each predicted TMD in the closely related poliovirus 2B protein. We have compared the capacity of 2B hairpin-derived peptides to insert into lipid monolayers and lyse unilamellar vesicles made of PI or PC lipids and subsequently characterized the structures responsible for the observed effects. We found distinct structures in TM1−TM2 mixtures under conditions of positive synergy in anionic membrane permeabilization. Thus, our data support the idea that N-terminal TMD cytolytic activity requires the cooperation of the C-terminal TMD to evolve in the context of anionic membranes targeted by 2B. We surmise that translocation across the bilayer of the amphipathic TM1 and the highly polar connecting short turn involves association with the highly conserved TM2 sequence, which subsequently takes part in the membrane permeating 2B pore assembly.

MATERIALS AND METHODS

Materials. The poliovirus 2B-derived peptides listed in Table 1 were produced by solid-phase synthesis using Fmoc chemistry as C-terminal carboxamides and purified by high-performace liquid chromatography (HPLC). Melittin and cecropin A were purchased from Bachem (Bubendorf, Switzerland). Plasmids encoding MBP−2B fusion proteins were constructed by subcloning poliovirus 2B-encoding DNA into the pMALc2 vector (New England Biolabs Inc., Beverly, MA). The constructs were expressed in *Escherichia coli* BL21pLys(DE3) as the host strain and purified as previously described (*13*). Phosphatidylcholine (PC) and phosphatidylinositol (PI) were purchased from Avanti Polar Lipids (Birmingham, AL). The 8-aminonaphthalene-1,3,6-trisulfonic acid sodium salt (ANTS) and *p*-xylenebis(pyridinium)bromide (DPX) were obtained from Molecular Probes (Junction City, OR). All other reagents were analytical grade.

Lipid Monolayer Assays. For the monolayer penetration assays, surface pressure was determined in a fixed-area circular trough (μTrough S system, Kibron) measuring 2 cm in diameter with a volume of 1 mL. The aqueous phase consisted of 1 mL of 5 mM Hepes and 100 mM NaCl (pH 7.4). Lipids, dissolved in chloroform, were spread over the surface, and the desired initial surface pressure (π_0) was attained by changing the amount of lipid applied to the air−water interface. Peptides were injected into the subphase with a Hamilton microsyringe to a final concentration of 0.5 μM. At this concentration, the peptides alone induced a negligible increase in surface pressure at the air−water interface.

Lipid Vesicle Assays. Large unilamellar vesicles (LUV) made of PI or PC were prepared according to the extrusion method in 5 mM Hepes and 100 mM NaCl (pH 7.4) using membranes with a nominal pore size of 0.1 μm. Vesicle permeabilization was assayed by monitoring the release to the medium of encapsulated fluorescent ANTS [ANTS/DPX assay (*22*)]. LUV containing 12.5 mM ANTS, 45 mM DPX, 20 mM NaCl, and 5 mM Hepes were obtained by separating the unencapsulated material by gel filtration in a Sephadex G-75 column that was eluted with 5 mM Hepes and 100 mM NaCl (pH 7.4). Fluorescence measurements were performed by setting the ANTS emission at 520 nm and the excitation at 355 nm. A cutoff filter (470 nm) was placed between the sample and the emission monochromator. The baseline leakage (0%) corresponded to the fluorescence of the vesicles at time zero, while 100% leakage was the fluorescence value obtained after addition of Triton X-100 (0.5%, v/v).

Circular Dichroism. Circular dichroism (CD) measurements were obtained from a thermally controlled Jasco J-810 circular dichroism spectropolarimeter calibrated routinely with (1*S*)-(+)-10-camphorsulfonic acid, ammonium salt. Stock peptide samples consisted of single sequences or mixtures preincubated in DMSO, lyophilized, and finally dissolved in 2 mM Hepes (pH 7.4) buffer at concentrations of 0.03 mM. Spectra were recorded in a 1 mm path length quartz cell initially equilibrated at 25 °C. Data were taken with a 1 nm bandwidth at a speed of 20 nm/min, and the results of five scans were averaged.

Antimicrobial and Hemolytic Activity. Inhibition of *E. coli* (BL21) and *Bacillus subtilis* (1A700) growth and human erythrocyte lysis induced by the peptides were assessed essentially as described by Oren et al. (*23*). In brief, for the antimicrobial assay, peptides dissolved in water (50 μL) were mixed with bacterial inoculums (50 μL containing bacteria at a concentration of 10^6 colony-forming units/mL in Luria-Bertani culture medium) in a 96-well microtiter plate. All

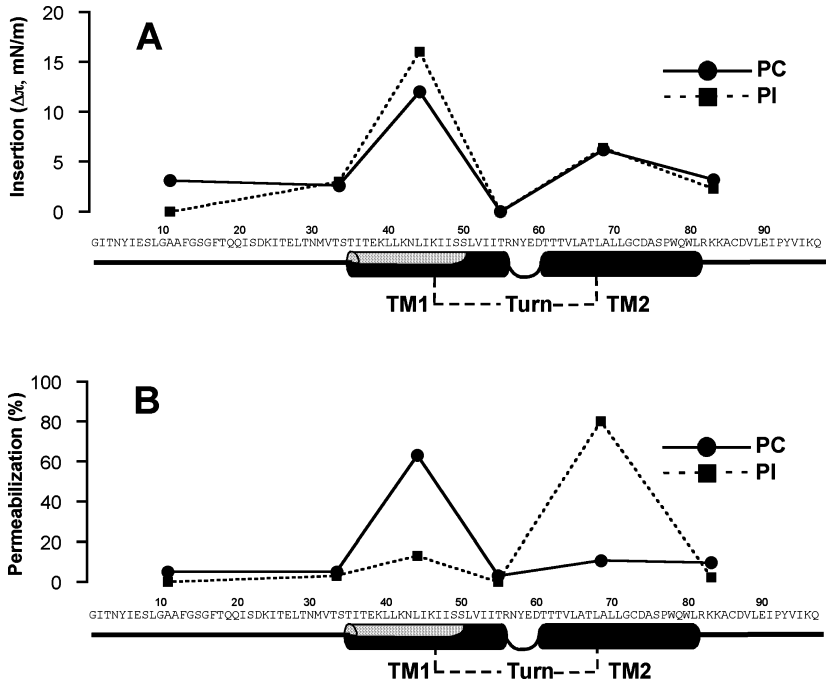

FIGURE 1: Membrane activity of the PV-1 2B sequence-derived peptide library. (A) Capacities of insertion of the peptides into PC and PI monolayers (● and ■, respectively). The values represent the maximal lateral pressure increases registered upon injection of the peptide into the subphase of lipid monolayers compressed at an initial pressure of 25 mN/m. (B) Levels of PC and PI LUV permeabilization (● and ■, respectively). Extents of ANTS leakage after peptide/LUV incubation for 30 min were determined at a 10^3:1 lipid:peptide molar ratio (lipid concentration, 50 μM). In both panels, mean values of two independent experiments are plotted for the center amino acid in each sequence depicted in Table 1.

peptides were tested in duplicate. The microtiter plates were incubated in a shaker overnight at 37 °C, and the absorbance at 620 nm was measured in a Synergy HT microplate reader (Bio-TEK Instruments Inc.). The growth inhibition percentage was calculated relative to growth in the absence of the test peptides.

Hemolysis assays were performed in duplicate by mixing 50 μL of a 5% suspension of freshly drawn human erythrocytes and 50 μL of the peptides dissolved in an isosmotic buffer. After incubation at 37 °C for 30 min under agitation, the samples were centrifuged (800*g* for 10 min). Supernatants were transferred into a 96-well microtiter plate, and absorbance was measured in the microplate reader at 412 nm. Complete hemolysis was assessed in samples containing 1% (v/v) Triton X-100.

RESULTS

Activity of the 2B Peptide Library in PI and PC Model Membranes. Figure 1 displays the capacities to insert and lyse model membranes of the PV 2B sequence-derived peptides listed in Table 1. Panel A compares insertion of the peptide into PC or PI monolayers initially compressed to ≈25 mN/m. An increase in the lateral pressure of both uncharged (●) and anionic (■) lipid monolayers was prominently induced by the TM1 peptide spanning the partially amphipathic N-terminal transmembrane domain. Although to a lesser degree, the TM2 peptide representing the second transmembrane domain also induced increases in lateral pressures consistent with its efficient insertion into both types of monolayers. By comparison, the rest of the peptides inserted less efficiently. The lytic activity of the library assayed in LUV (added at a lipid-to-peptide ratio of 10^3:1) revealed a contrasting behavior in PC and PI vesicles (Figure 1B). Thus, TM1 induced extensive release of aqueous contents from PC vesicles (●) but did not permeabilize PI liposomes efficiently (■). In contrast, TM2 induced leakage of ANTS from PI vesicles very efficiently but barely affected the uncharged ones. Interestingly, the "Turn" peptide, which combines the predicted short connecting sequence and the hydrophobic residues of both TMDs, was inactive in both systems. The rest of the peptides did not induce significant leakage from liposomes. In conclusion, the results displayed in Figure 1 support the fact that the predicted TMDs are directly involved in insertion of 2B protein into membranes and in the establishment of permeating pores therein. However, they also indicate that membranolytic activity is distinctly distributed along the hairpin element. Thus, an alternative hypothesis could be that TM1 is the active domain in neutral lipids, while TM2 is the active domain in anionic lipids. Nonetheless, the fact that both domains are required for the stable insertion of the 2B protein into target organelles and the process of membrane permeabilization (*15*) suggests that TM1 might also play a role in the permeabilization of the negatively charged membranes. Our analysis supports this latter possibility.

Membrane Interactions of TM1, Turn, TM2, and Complete 2B. To establish the relative importance of the transmembrane hairpin sequences in 2B insertion and pore forming activity, we further characterized TM1, Turn, and TM2 in their capacity to interact with PI and PC model membranes (Figures 2 and 3). The membrane activity displayed by the MBP-2B construct was included as a reference in this analysis. Figure 2 compares the capacity of the peptides and full protein to insert into lipid monolayers. The critical pressures for insertion (i.e., the surface pressure at which the sequences were excluded from the lipid monolayer, π_c)

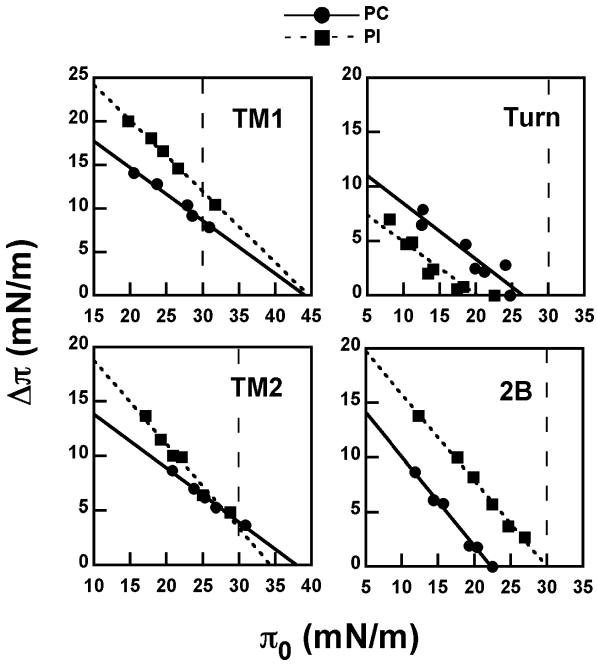

FIGURE 2: Membrane insertion capacities of 2B and 2B hairpin-derived peptides. The maximum increase in surface pressure induced by TM1, Turn, TM2, or MBP-2B was measured as a function of the initial surface pressure of PC and PI phospholipid monolayers (● and ■, respectively). The dashed lines begin at 30 mN/m.

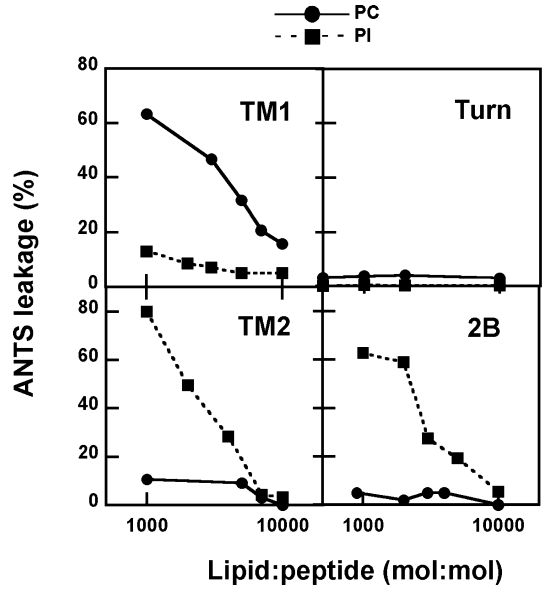

FIGURE 3: Permeabilization of lipid vesicles by 2B and 2B hairpin-derived peptides. Extents of ANTS leakage were measured after incubation of TM1, Turn, TM2, or MBP-2B with PC or PI LUV for 30 min as a function of the lipid:peptide molar ratio (● or ■, respectively). The lipid concentration was 50 μM in all cases.

indicated that TM1 and TM2 were capable of penetrating into PC and PI monolayers at the surface pressures present in unstressed natural membranes [$\pi_c \geq 30$ mN/m (*24*)]. Conversely, the Turn peptide was predicted not to insert into natural 2B target membranes. Finally, the data confirmed the insertion of the complete 2B protein into PI monolayers slightly compressed above 30 mN/m, but not into PC monolayers compressed above 22.5 mN/m.

Figure 3 compares the lytic activities of peptides and protein measured in LUV. Within the 10^3:1 to 10^4:1 lipid:peptide ratio range, TM1 induced leakage from PC, but barely from PI vesicles. The reverse was true for TM2, while the Turn peptide exhibited no effect on vesicle permeability. Consistent with its monolayer penetrating capacity, the complete 2B protein induced leakage only from PI vesicles. Thus, the data shown in Figure 3 demonstrate that in the range of concentrations tested, only TM2 reproduced the lytic activity of the complete protein.

Table 2: Secondary Structure Fractions Estimated from CDPro (*41*)[a]

condition	structure	TM1	Turn	TM2
solution	helix	0.205	0.031	0.062
		0.201	−	0.036
		−	0.049	−
	strand	0.188	0.323	0.370
		0.232	−	0.372
		−	0.307	−
	turn	0.228	0.160	0.231
		0.229	−	0.234
		−	0.253	−
	unordered	0.379	0.487	0.337
		0.345	−	0.347
		−	0.349	−
SDS[b]	helix (r/d)	0.442	0.041	0.407
		0.426	0.050	0.250
		0.466	0.026	0.237
	strand (r/d)	0.120	0.327	0.318
		0.161	0.287	0.223
		0.125	0.307	0.252
	turn	0.155	0.177	0.063
		0.147	0.067	0.210
		0.144	0.159	0.195
	unordered	0.283	0.455	0.213
		0.276	0.538	0.287
		0.264	0.492	0.309

[a] Fractions estimated with CONTIN-LL, CDSSTR, and SELCON3 (first, second, and third values per structure, respectively). The SMP-56 reference protein set provided by the software was used for calculating the reconstructed spectra. [b] CD measurements reported in ref *20*.

Structural Characterization of TM1, Turn, and TM2 in Membranes. The peptide structures associated with the promotion of the observed lytic effects were characterizad by circular dichroism (CD). A quantitative CD analysis of the secondary structure composition was performed for peptide spectra measured in solution, membrane mimetic SDS micelles, and lipid vesicles (Tables 2 and 3 and Figure 4). As reported in our previous work (*20*), the TM1 α-helical conformation has been detected in solution and became predominant in membrane-mimetic SDS micelles, where the turn+unordered structure still accounted for a comparable but lower fraction of structure (Table 2). The Turn sequence remained essentially unstructured in solution and SDS micelles. TM2 structuring was also promoted when it dispersed in SDS, but in this case, helices and extended strands accounted for quantitatively similar structure fractions.

The addition of lipid vesicles also affected the structures adopted by the peptides (Figure 4 and Table 3). In the presence of PC vesicles, the TM1 peptide exhibited mainly helix and turn+unordered structures whose fractions were overall comparable to those measured in the SDS-containing medium. In contrast, the α-helical conformation was predominant in the presence of PI vesicles (fraction of ≈0.85) (Figure 4 and Table 3). By comparison, the Turn peptide CD spectra denoted an absence of secondary structure induction in the presence of PC or PI vesicles (Figure 4). CD spectra measured for TM2 in the presence of PC vesicles

Table 3: Secondary Structure Fractions Estimated from the CD Spectra Displayed in Figure 4 Using CDPro (*41*)[a]

condition	structure	TM1	Turn	TM2
PC	helix (r/d)	0.448	0.027	0.112
		0.438	−	0.104
		0.521	0.024	0.065
	strand (r/d)	0.069	0.337	0.314
		0.145	−	0.457
		0.081	0.401	0.330
	turn	0.162	0.164	0.233
		0.175	−	0.204
		0.124	0.215	0.253
	unordered	0.321	0.471	0.342
		0.263	−	0.198
		0.285	0.324	0.343
PI	helix (r/d)	0.801	0.002/0.031	0.212
		0.813	−/−	0.202
		0.883	0.000/0.016	0.208
	strand (r/d)	0.014	0.202/0.115	0.288
		0.000	−/−	0.283
		0.032	0.194/0.107	0.300
	turn	0.066	0.160	0.206
		0.051	−	0.213
		0.025	0.182	0.203
	unordered	0.119	0.490	0.303
		0.143	−	0.309
		0.046	0.484	0.287

[a] Fractions estimated with CONTIN-LL, CDSSTR, and SELCON3 (first, second, and third values per structure, respectively). The SMP-56 reference protein set provided by the software was used for calculating the reconstructed spectra.

exhibited negative bands centered at ≈202−205 nm and negative shoulders at ≈224 nm (Figure 4). Those spectra might denote an important contribution of type I β-turn conformers (*25*) and/or type II β-rich protein structures (*26*). Accordingly, the analysis of the secondary structure composition revealed that strands and turns accounted for the majority of the periodic structures in the TM2 spectrum, while helices contributed less (Table 3). Finally, the minimum shifted to 217 nm, together with band components at 208 and 222 nm, suggests that the mixture of helical and extended β-type strands accounted for the major fraction of the structure adopted by this peptide in the presence of PI vesicles (Table 3).

Synergism in Membrane Permeabilization. The preceding results indicate that a TM1 helix inserted into PI membranes would be not functional in pore opening, while TM2 adopting a comparatively higher proportion of nonhelical structures would be lytic for the same membranes. Data displayed in Figures 5−7 support a concerted action of both domains in 2B pore opening in anionic PI membranes. As stated before, TM1 induced efficient release of aqueous contents from PC vesicles at a lipid:peptide ratio of 10^3:1 (Figure 5, top panel). By comparison, TM2 induced much less ANTS leakage, in terms of both final extents and initial rates (inset). Simultaneous addition of both peptides in a 1:1 mixture resulted in slightly lower rates and extents compared to those with TM1 alone, which was consistent with the existence of subtle interference. In contrast to this situation, TM1 induced almost no aqueous content leakage when added to PI LUV, while incubation of these vesicles with TM2 resulted in extensive internal marker release (bottom panel). In this case, addition of both peptides from the 1:1 mixture resulted in much faster (inset) and more extensive release of ANTS into the medium. This effect clearly supported the existence of a positive synergism in the permeabilization of PI vesicles.

Data displayed in Figure 6 illustrate the effect of pre-adding increasing doses of TM2 to PC (●) and TM1 to PI (■) vesicles on the extent of leakage induced by TM1 and TM2, respectively. TM1-induced leakage from the PC vesicles was slightly inhibited by TM2. In contrast, TM2-induced leakage from the PI vesicles was significantly enhanced by TM1 pre-addition. In this case, leakage was maximal at a ca. 1:1 TM1:TM2 molar ratio. Further CD characterization of the equimolar TM1/TM2 mixtures indeed revealed the formation of distinct structures in membranes (Figure 7). A comparison of the experimental spectra (solid lines) and those calculated for the addition of noninteracting peptide signals (dotted lines) indicated that TM1 and TM2 in solution or dispersed in SDS adopted comparable structures as isolated species or in mixtures (panel A, top). However, the same comparison revealed a certain degree of conformational rearrangement in the TM1/TM2 mixtures incubated with PC LUV (panel A, bottom left), and, more prominently, in those incubated with PI LUV (panel A, bottom right). The experimental spectrum obtained in the presence of PC vesicles displayed a weaker negative band shifted toward higher wavelengths, which correlated with a significant reduction in the level of unordered and turn structures and a subtle increase in the content of extended β-type strands (panel B). In the presence of PI vesicles, the measured experimental spectrum disclosed a positive band shifted toward lower wavelengths and weaker negative absorption. Analysis of the secondary structure composition revealed a significant reduction in the helicity of the TM1/TM2 mixture concomitant with an increase in extended β-type strands and unordered structures (panel B).

Thus, the CD signals derived from the mixtures in the presence of the anionic PI vesicles suggest that TM1 and TM2 co-assembled into a complex containing a high proportion of nonhelical structures. Interestingly, the helicity reduction correlated in this system with an increase in the observed lytic potency (Figures 5 and 6).

TM1 and TM2 Activity in Natural Membranes. Given the fact that TM1 could induce nonselective pores in cells, in our previous report (*20*) we suggested that 2B viroporin might be functionally homologous to cytolytic pore-forming proteins and peptides targeting the plasma membrane of animal cells. Results in this work indicate that TM2 also exerted a lytic effect, mainly restricted to anionic membranes. Selective lysis of anionic membranes versus uncharged ones is a hallmark of antimicrobial peptides, while cytolytic peptides tend to exhibit lower membrane selectivity (*27, 28*). Thus, the selectivity observed in vesicles (Figure 3) suggested that TM1 and TM2 might exhibit cytolytic and antimicrobial activities, respectively. We therefore assessed their capacity to arrest bacterial growth and to lyse erythrocytes as standard measurements of these activities (Figure 8).

Supporting its cytolytic character, TM1 exhibited a hemolytic activity comparable to that of melittin, which was used as a positive control in our studies (IC_{50} values of ca. 8 and 4 μM, respectively). Consistent with the existence of interference also in this system, the equimolar TM1/TM2 mixture induced hemolysis to a lower extent ($IC_{50} > 50\ \mu M$). No TM2 activity could be detected at the assayed concentrations. In contrast to the hemolysis results, none of the viral peptides exhibited an antimicrobial activity comparable to that of cecropin A used as a positive control. However, at

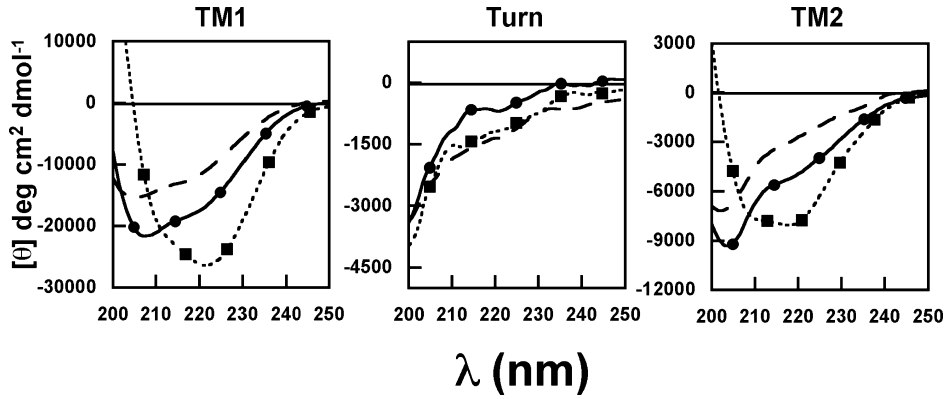

FIGURE 4: Structure of 2B hairpin-derived peptides in the presence of lipid vesicles. CD spectra of TM1, Turn, and TM2 peptides were obtained in buffer (dashed lines) and in the presence of 1 mM PC or PI vesicles (● or ■, respectively).

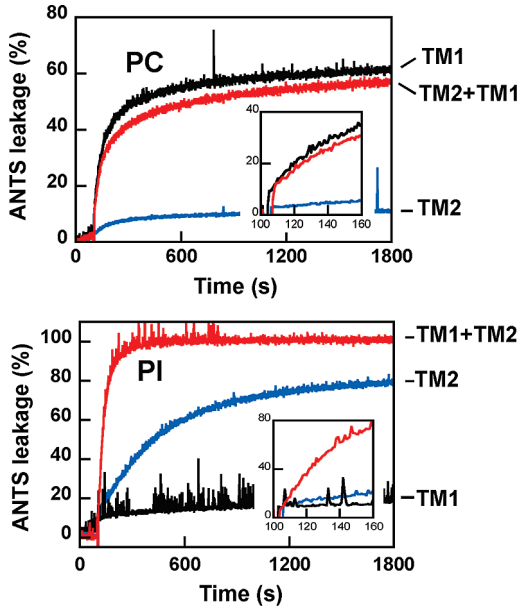

FIGURE 5: Synergism in membrane permeabilization. TM1 (black traces), TM2 (blue traces), or the equimolar TM1/TM2 mixture (red traces) was added at a final 10^3:1 lipid:peptide molar ratio to PC and PI vesicles (top and bottom panels, respectively). Peptides were added to liposomes after 100 s, and the resulting ANTS leakage was continuously monitored as a function of time. The insets show the initial rates of the process.

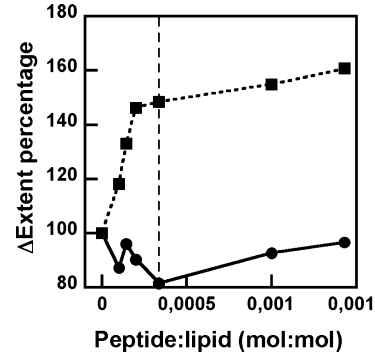

FIGURE 6: Effect of peptide pre-addition on membrane permeabilization. In these experiments, TM2 and TM1 were pre-added to PC (●) and PI (■) vesicles, respectively, at the indicated peptide: lipid ratios. After incubation for 1 min, the PC/TM2 and PI/TM1 mixtures were supplemented with TM1 and TM2, respectively, added at a fixed 1:3000 peptide:lipid molar ratio (dose indicated by the dashed line). Extents of ANTS release after 30 min are plotted. The final extent in the absence of pre-added peptide was set to 100%.

the highest tested concentration of 50 μM, TM2 or the TM1/TM2 mixture induced partial growth inhibition of *E. coli* (by ≈50%). This effect might be significant since a similar treatment did not affect *B. subtilis* growth to the same extent.

In summary, the results obtained in natural membrane systems reinforce the notion that TM1 sequence bears a cytolytic activity. However, none of these virally encoded sequences efficiently inhibited bacterial growth. These observations correlate with TM1 and TM2 membrane activities being specifically required for effective 2B-induced pore formation in the context of target organelle permeabilization.

DISCUSSION

The nonstructural 2B and 2BC proteins are known to exert membrane regulatory functions during enterovirus and rhinovirus replicative cycles, which apparently are not shared by other members of the Picornaviridae family (*2, 29*). The precise physiological role played by the various 2B membrane activities is still a matter of investigation. Upon expression, the 2B protein has been shown to localize mainly in the ER and Golgi complex, a phenomenon linked with a decrease in calcium and proton levels in the lumens of these organelles (*4, 5, 7*−*9*). It has been hypothesized that 2B-induced permeabilization results in downregulation of Ca^{2+} signaling to mitochondria and therefore prevents apoptosis at early stages of the infectious cycle (*8*). In addition, PV 2B also localizes partially in mitochondria and induces an anomalous perinuclear distribution of these organelles when expressed from a Sindbis replicon (*10*). The detection of the release of cytochrome *c* from mitochondria linked to the high 2B expression levels suggests that this protein may induce apoptosis via the mitochondrial pathway in the late phases of infection. Carrasco and co-workers (*10*) suggested that this dual role of 2B in regulating cell death may be physiologically significant for viral replication: at early phases by preventing the blocking of efficient viral gene expression and protein synthesis and at late phases of infection by preventing host immune inflammatory responses.

Biochemical evidence obtained in model membranes devoid of other cellular factors supports the intrinsic capacity of the 2B moiety to directly permeabilize cell endomembranes (*13*). Several features of the vesicle permeabilization process, including the small doses required for the promotion of the effective release of the aqueous contents (in the order of one added protein per 10^4 lipids), the fact that the activity is specific for

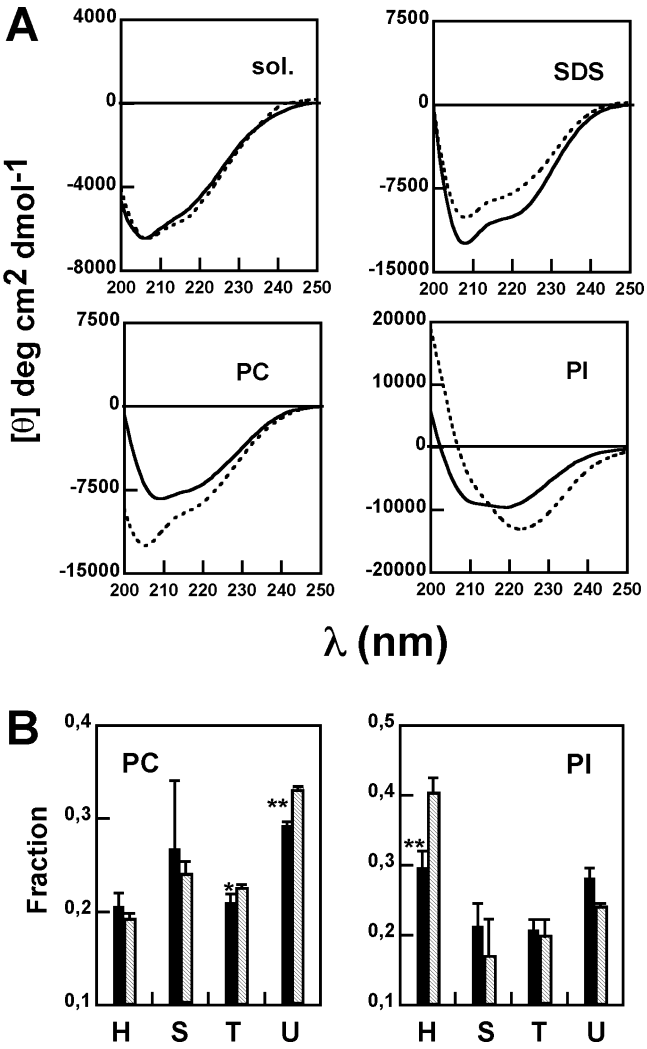

FIGURE 7: Assembly of TM1 and TM2 sequences as determined by CD. (A) Spectra of an equimolar TM1/TM2 mixture (solid lines) in different media, as indicated in the panels. The dotted lines are the spectra calculated by adding the corresponding individual TM1 and TM2 signals. (B) Comparison of the structural components calculated for the spectra obtained in the presence of PC and PI vesicles. Means ± the standard deviation for the fraction values estimated with CONTIN-LL, CDSSTR, and SELCON3 are plotted for experimental (black bars) and added individual CD spectra (hatched bars). H, helix; S, strand; T, turns; U, unordered. For the experimental mixtures, a significant decrease was observed in the level of helical conformation in PI and unordered structures and turns in PC (**$p < 0.005$; *$p < 0.05$).

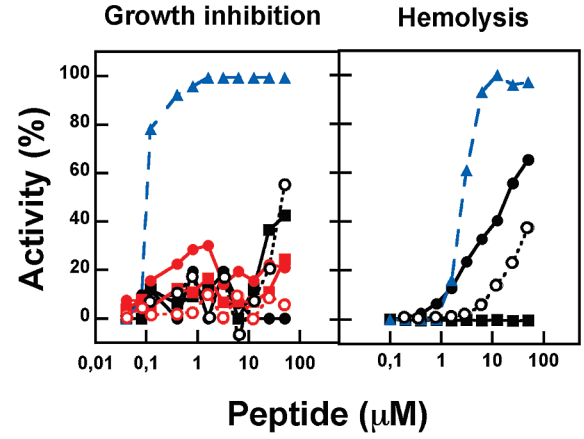

FIGURE 8: Dose−response curves of antimicrobial (left panel) and hemolytic activities (right panel): (●) TM1, (■) TM2, (○) and TM1/TM2 (1:1) mixture. In the left panel, inhibition of *E. coli* (Gram-negative) and *B. subtilis* (Gram-positive) growth is indicated by the black and red symbols, respectively. Blue triangles correspond to cecropin A-induced *E. coli* growth inhibition and melittin-induced hemolysis in the left and right panels, respectively.

low-molecular weight solutes, and the stability of the established permeating structures, all support pore formation as the likely mechanism sustaining 2B-induced organelle permeabilization. Also supporting a pore forming mechanism, 2B shares structural similarities with the pro-apoptotic members of the BCL-2 family (*30*), and certain cytolytic toxins (*31, 32*). Members of these protein families include similar α-helix−turn−α-helix membrane anchor motifs postulated to be actively involved in porating the lipid bilayer (*16, 33*−*38*).

In this and previous work, we have used a peptide-based analysis to examine the functional roles played by the predicted hairpin constituents in 2B permeabilizing activity. TM1 externally added to cells reproduced the plasma membrane permeabilization phenomenon observed upon intracellular expression of complete 2B (*20*). In line with its capacity to interact with electrically neutral membrane surfaces, this peptide induced leakage of contents from PC vesicles in the 10^3:1 to 10^4:1 lipid:peptide ratio range and erythrocyte lysis. By comparison, TM1 permeabilizing activity was restrained in anionic PI vesicles, and its addition to the culture medium did not affect bacterial growth. In contrast, TM2 did not induce significant plasma membrane permeabilization and had little effect on the stability of uncharged PC vesicles but efficiently perturbed anionic PI vesicles.

Thus, the relatively low TM1 lytic activity measured in PI vesicles primarily suggests that this sequence is not functional in pore formation at the surface of negatively charged organelle membranes. However, TM1 inserted efficiently and became highly structured in anionic PI membranes. We infer that the low lytic activity of helix TM1 inserted into the anionic membranes might be due to favorable electrostatic interactions between positively charged Lys residues and negatively charged polar headgroup moieties. A strong electrostatic interaction might anchor this sequence to the membrane interface, a phenomenon described to occur in the case of antimicrobial cationic peptides interacting with anionic membranes (*27, 28*). In addition, the experimental data indicate that the presence of the highly polar RNYED sequence is sufficient to impair Turn peptide structuring and membrane interactions. It can be inferred that for both factors, translocation across the bilayer of the highly polar turn region and the favorable TM1−phospholipid interfacial interactions are likely to restrain 2B hairpin insertion and its subsequent assembly into a membrane pore.

Our results actually support the possibility that TM2 might play a crucial role in the 2B pore formation mechanism by unleashing these constraints. The capacity to insert into and lyse PI vesicles suggests that this sequence might participate in the assembly of a permeating structure. Interestingly, TM2 retained a high proportion of extended structures in the presence of PI vesicles or when dispersed in membrane-mimic SDS. Moreover, the positive TM1−TM2 synergy detected in PI vesicles would be consistent with the recruitment of interface-adsorbed TM1 into mixed TM1−TM2 pores. Consistent with this mechanism, equimolar TM1/TM2 mixtures adopt in the presence of PI membranes distinct structures with reduced helicity.

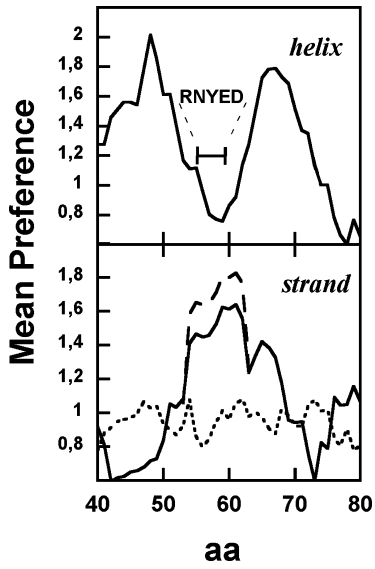

FIGURE 9: Scores of transmembrane secondary structure preferences within the 2B hairpin sequence. In the top panel, an 11-residue sliding window was used to calculate the means of the preference [$P\alpha$(TM)] values of the individual amino acids for their occurrence in a transmembrane helix as reported by Liu and Deber (*39*). In the bottom panel, a nine-residue sliding window was used to calculate mean values of normalized amino acid abundance in bilayer-embedded β-barrel strands as reported by Wimley (*40*). Following the work of this author, the two possible frames within a strand sequence were considered in the calculations, i.e., placing interior (barrel-facing) and exposed (lipid-facing) abundance data values in alternating positions (solid and dotted lines). The slashed stretch was calculated using normalized values for RNEYD abundance in membrane β-barrels at the interface level.

Plots displayed in Figure 9 support the possibility that the 2B transmembrane hairpin might include residues adopting extended structures. Those plots score sequences showing a propensity to traverse the bilayer in a given conformation. To produce them, we used the values for the preferences of the individual amino acids for their occurrence in transmembrane helices and extended strands, reported by Liu and Deber (*39*) and Wimley (*40*), respectively. When the mean preference of 2B hairpin amino acids for the occurrence in a transmembrane helix was calculated (top panel), the plot revealed the presence of two peaks spanning TM1 and TM2 regions and a minimum between them, which corresponded to the RNYED short turn. Conversely, a single peak was observed when calculations were performed using normalized bilayer abundances in strands of β-barrel membrane proteins (bottom panel). Following Wimley (*40*), in this case mean values were calculated either for lipid-facing/interior-facing or for interior-facing/lipid-facing dyad repeats (solid and dotted lines, respectively). The presence of a peak above 1 for only one of the dyad repeats strengthens the structural significance of the accumulation within the 2B hairpin of ca. 20 amino acids that are abundant in transmembrane β-strands. This continuous, in-frame stretch spanned the carboxy terminus of TM1, the connecting short turn, and the amino-terminal end of TM2. The peak gained intensity when for the same dyad repeat, normalized abundance values at the membrane interface were applied to the RNYED residues, suggesting that this element might also play a role as an interstrand loop.

The 2B hairpin-insertion model depicted in Figure 10 summarizes these predictions and the previously reported experimental observations. We propose that the initial interaction of the 2B or 2BC precursor with negatively

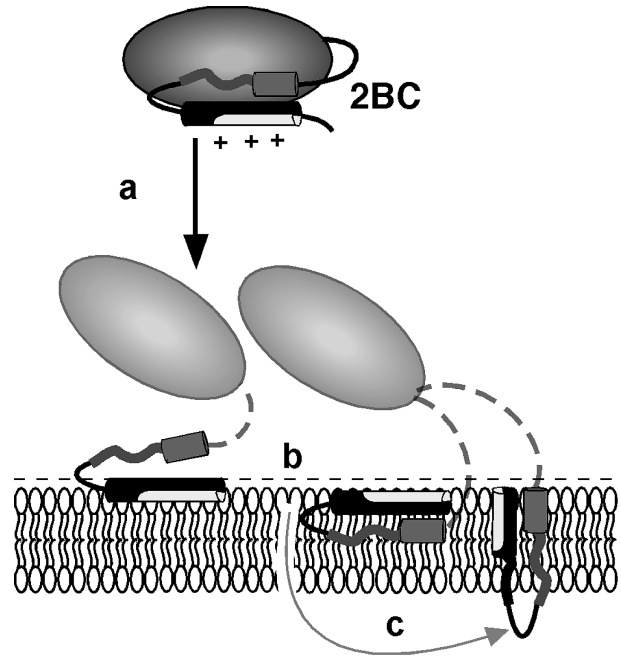

FIGURE 10: Model for insertion of the 2B hairpin into target organelles. See Discussion for details.

charged endomembrane surfaces might be based on favorable electrostatic interactions, most likely mediated by the positively charged surface of a preformed TM1 helical stretch (a). This interaction results in the stabilization of the TM1 helix at the membrane interface (b). Formation of a complex with TM2 most likely confers the flexibility and hydrophobicity distribution required to allow translocation of TM1 and connecting polar turn across the bilayer (c). Consistent with this idea, the measured and predicted transmembrane structures suggest that the translocated hairpin region might include a significant proportion of extended structures. However, we caution that, due to amide H-bonding requirements, extended chains are unlikely to traverse the membrane in a monomer like the one depicted in the model of Figure 10. Thus, it is inferred that these H-bonding requirements are probably fulfilled within the oligomeric 2B pore structures (not shown in the model). We previously also argued that TM1 translocation and the opening of a permeating pore would be causally linked due to the necessity of orienting charged Lys residues toward the water-filled lumen (*14*).

In conclusion, our peptide-based analysis is consistent with previous mutagenesis studies, which indicated that both 2B TMDs cooperate in permeabilizing cell target membranes (*15*), and provides new insights into the molecular mechanism underlying this phenomenon. The data confirm the cytolytic activity of the amino-terminal TMD and support unforeseen functions for the mildly hydrophobic carboxy-terminal TMD, which is highly conserved in and between enterovirus and rhinovirus genera. Thus, we postulate that the TM2 domain might directly take part in the assembly of permeating pores but also be required for the translocation of the cytolytic TM1 and the polar connecting turn. We speculate that the latter process might constitute the limiting step in the spontaneous insertion of the hairpin into cell organelles. Finally, our data indicate that the permeating oligomeric 2B pore could be structurally more complex than the assumed ensemble of transmembrane helices.

REFERENCES

1. Carrasco, L., Perez, L., Irurzun, A., Martinez-Abarca, F., Rodriguez, P., Guinea, R., Castrillo, J. L., Sanz, M. A., and Ayala, M. J. (1993) Modification of membrane permeability by animal viruses. In *Regulation of Gene Expression in Animal Viruses* (Carrasco, L., Sonenberg, N., and Wimmer, E., Eds.) pp 283−305, Plenum Press, London.
2. de Jong, A. S., de Mattia, F., Van Dommelen, M. M., Lanke, K., Melchers, W. J., Willems, P. H., and van Kuppeveld, F. J. (2008) Functional analysis of picornavirus 2B proteins: Effects on calcium homeostasis and intracellular protein trafficking. *J. Virol. 82*, 3782–3790.
3. Aldabe, R., Barco, A., and Carrasco, L. (1996) Membrane permeabilization by poliovirus proteins 2B and 2BC. *J. Biol. Chem. 271*, 23134–23137.
4. Aldabe, R., Irurzun, A., and Carrasco, L. (1997) Poliovirus protein 2BC increases cytosolic free calcium concentrations. *J. Virol. 71*, 6214–6217.
5. van Kuppeveld, F. J., Hoenderop, J. G., Smeets, R. L., Willems, P. H., Dijkman, H. B., Galama, J. M., and Melchers, W. J. (1997) Coxsackievirus protein 2B modifies endoplasmic reticulum membrane and plasma membrane permeability and facilitates virus release. *EMBO J. 16*, 3519–3532.
6. Carrasco, L., Guinea, R., Irurzun, A., and Barco, A. (2002) Effects of viral replication on cellular membrane metabolism and function. In *Molecular biology of picornavirus* (Semler, B. L., and Wimmer, E., Eds.) pp 337−354, American Society for Microbiology Press, Washington, DC.
7. de Jong, A. S., Melchers, W. J., Glaudemans, D. H., Willems, P. H., and van Kuppeveld, F. J. (2004) Mutational analysis of different regions in the coxsackievirus 2B protein: Requirements for homomultimerization, membrane permeabilization, subcellular localization, and virus replication. *J. Biol. Chem. 279*, 19924–19935.
8. de Jong, A. S., Visch, H. J., de Mattia, F., van Dommelen, M. M., Swarts, H. G., Luyten, T., Callewaert, G., Melchers, W. J., Willems, P. H., and van Kuppeveld, F. J. (2006) The coxsackievirus 2B protein increases efflux of ions from the endoplasmic reticulum and Golgi, thereby inhibiting protein trafficking through the Golgi. *J. Biol. Chem. 281*, 14144–14150.
9. Sandoval, I. V., and Carrasco, L. (1997) Poliovirus infection and expression of the poliovirus protein 2B provoke the disassembly of the Golgi complex, the organelle target for the antipoliovirus drug Ro-090179. *J. Virol. 71*, 4679–4693.
10. Madan, V., Castello, A., and Carrasco, L. (2008) Viroporins from RNA viruses induce caspase-dependent apoptosis. *Cell. Microbiol. 10*, 437–451.
11. van Kuppeveld, F. J., Galama, J. M., Zoll, J., van den Hurk, P. J., and Melchers, W. J. (1996) Coxsackie B3 virus protein 2B contains cationic amphipathic helix that is required for viral RNA replication. *J. Virol. 70*, 3876–3886.
12. van Kuppeveld, F. J., Melchers, W. J., Kirkegaard, K., and Doedens, J. R. (1997) Structure-function analysis of coxsackie B3 virus protein 2B. *Virology 227*, 111–118.
13. Agirre, A., Barco, A., Carrasco, L., and Nieva, J. L. (2002) Viroporin-mediated membrane permeabilization. Pore formation by nonstructural poliovirus 2B protein. *J. Biol. Chem. 277*, 40434–40441.
14. Nieva, J. L., Agirre, A., Nir, S., and Carrasco, L. (2003) Mechanisms of membrane permeabilization by picornavirus 2B viroporin. *FEBS Lett. 552*, 68–73.
15. de Jong, A. S., Wessels, E., Dijkman, H. B., Galama, J. M., Melchers, W. J., Willems, P. H., and van Kuppeveld, F. J. (2003) Determinants for membrane association and permeabilization of the coxsackievirus 2B protein and the identification of the Golgi complex as the target organelle. *J. Biol. Chem. 278*, 1012–1021.
16. Gazit, E., La Rocca, P., Sansom, M. S., and Shai, Y. (1998) The structure and organization within the membrane of the helices composing the pore-forming domain of *Bacillus thuringiensis* δ-endotoxin are consistent with an "umbrella-like" structure of the pore. *Proc. Natl. Acad. Sci. U.S.A. 95*, 12289–12294.
17. Shai, Y. (1995) Molecular recognition between membrane-spanning polypeptides. *Trends Biochem. Sci. 20*, 460–464.
18. Stouffer, A. L., Nanda, V., Lear, J. D., and DeGrado, W. F. (2005) Sequence determinants of a transmembrane proton channel: An inverse relationship between stability and function. *J. Mol. Biol. 347*, 169–179.
19. Ojcius, D. M., Persechini, P. M., Zheng, L. M., Notaroberto, P. C., Adeodato, S. C., and Young, J. D. (1991) Cytolytic and ion channel-forming properties of the N terminus of lymphocyte perforin. *Proc. Natl. Acad. Sci. U.S.A. 88*, 4621–4625.
20. Madan, V., Sanchez-Martinez, S., Vedovato, N., Rispoli, G., Carrasco, L., and Nieva, J. L. (2007) Plasma membrane-porating domain in poliovirus 2B protein. A short peptide mimics viroporin activity. *J. Mol. Biol. 374*, 951–964.
21. van Meer, G., Voelker, D. R., and Feigenson, G. W. (2008) Membrane lipids: Where they are and how they behave. *Nat. Rev. Mol. Cell Biol. 9*, 112–124.
22. Ellens, H., Bentz, J., and Szoka, F. C. (1985) H^+- and Ca^{2+}-induced fusion and destabilization of liposomes. *Biochemistry 24*, 3099–3106.
23. Oren, Z., Lerman, J. C., Gudmundsson, G. H., Agerberth, B., and Shai, Y. (1999) Structure and organization of the human antimicrobial peptide LL-37 in phospholipid membranes: Relevance to the molecular basis for its non-cell-selective activity. *Biochem. J. 341* (3), 501–513.
24. Marsh, D. (2007) Lateral pressure profile, spontaneous curvature frustration, and the incorporation and conformation of proteins in membranes. *Biophys. J. 93*, 3884–3899.
25. Perczel, A., and Fasman, G. D. (1992) Quantitative analysis of cyclic β-turn models. *Protein Sci. 1*, 378–395.
26. Sreerama, N., and Woody, R. W. (2004) Computation and analysis of protein circular dichroism spectra. *Methods Enzymol. 383*, 318–351.
27. Shai, Y. (1999) Mechanism of the binding, insertion and destabilization of phospholipid bilayer membranes by α-helical antimicrobial and cell non-selective membrane-lytic peptides. *Biochim. Biophys. Acta 1462*, 55–70.
28. Epand, R. M., and Vogel, H. J. (1999) Diversity of antimicrobial peptides and their mechanisms of action. *Biochim. Biophys. Acta 1462*, 11–28.
29. Gonzalez, M. E., and Carrasco, L. (2003) Viroporins. *FEBS Lett. 552*, 28–34.
30. Youle, R. J., and Strasser, A. (2008) The BCL-2 protein family: Opposing activities that mediate cell death. *Nat. Rev. Mol. Cell Biol. 9*, 47–59.
31. Parker, M. W., and Feil, S. C. (2005) Pore-forming protein toxins: From structure to function. *Prog. Biophys. Mol. Biol. 88*, 91–142.
32. Ojcius, D. M., and Young, J. D. (1991) Cytolytic pore-forming proteins and peptides: Is there a common structural motif? *Trends Biochem. Sci. 16*, 225–229.
33. Basanez, G., Sharpe, J. C., Galanis, J., Brandt, T. B., Hardwick, J. M., and Zimmerberg, J. (2002) Bax-type apoptotic proteins porate pure lipid bilayers through a mechanism sensitive to intrinsic monolayer curvature. *J. Biol. Chem. 277*, 49360–49365.
34. Epand, R. F., Martinou, J. C., Montessuit, S., and Epand, R. M. (2002) Membrane perturbations induced by the apoptotic Bax protein. *Biochem. J. 367*, 849–855.
35. Garcia-Saez, A. J., Coraiola, M., Serra, M. D., Mingarro, I., Muller, P., and Salgado, J. (2006) Peptides corresponding to helices 5 and 6 of Bax can independently form large lipid pores. *FEBS J. 273*, 971–981.
36. Terrones, O., Antonsson, B., Yamaguchi, H., Wang, H. G., Liu, J., Lee, R. M., Herrmann, A., and Basanez, G. (2004) Lipidic pore formation by the concerted action of proapoptotic BAX and tBID. *J. Biol. Chem. 279*, 30081–30091.
37. Masson, L., Tabashnik, B. E., Liu, Y. B., Brousseau, R., and Schwartz, J. L. (1999) Helix 4 of the *Bacillus thuringiensis* Cry1Aa toxin lines the lumen of the ion channel. *J. Biol. Chem. 274*, 31996–32000.
38. Sobko, A. A., Kotova, E. A., Antonenko, Y. N., Zakharov, S. D., and Cramer, W. A. (2006) Lipid dependence of the channel properties of a colicin E1-lipid toroidal pore. *J. Biol. Chem. 281*, 14408–14416.
39. Liu, L. P., and Deber, C. M. (1998) Uncoupling hydrophobicity and helicity in transmembrane segments. α-Helical propensities of the amino acids in non-polar environments. *J. Biol. Chem. 273*, 23645–23648.
40. Wimley, W. C. (2002) Toward genomic identification of β-barrel membrane proteins: Composition and architecture of known structures. *Protein Sci. 11*, 301–312.
41. Sreerama, N., and Woody, R. W. (2000) Estimation of protein secondary structure from circular dichroism spectra: Comparison of CONTIN, SELCON, and CDSSTR methods with an expanded reference set. *Anal. Biochem. 287*, 252–260.

BI800997A